Backscattering albedo contrast in OCT using plasmon-resonant gold nanorods

Amy L. Oldenburg[a], Matthew N. Hansen[b], Alexander Wei[b], Stephen A. Boppart[*a]
[a]Dept. of Electrical and Computer Engineering,
Beckman Institute for Advanced Science and Technology,
University of Illinois at Urbana-Champaign, 405 N. Mathews Ave., Urbana, IL, USA 61801;
[b]Dept. of Chemistry, Purdue University, 560 Oval Dr., West Lafayette, IN, USA 47907

ABSTRACT

Gold nanorods ~14 × 44nm exhibit a surface-plasmon resonance (SPR) peaked near 800nm which is dominated by absorption, not scattering. Because biological tissues in the near-infrared wavelength regime are predominantly scattering (high albedo), the addition of trace amounts of nanorods can be detected by their lowering of the albedo. Albedo is a preferred measurement parameter because it is insensitive to inhomogeneities in the density of scatterers. For optical coherence tomography (OCT) imaging applications, a related parameter called the backscattering albedo, equal to the ratio of the backscattering coefficient to the total extinction, is introduced for detecting gold nanorods. Here we use this parameter to investigate gold nanorods as contrast agents for optical coherence tomography (OCT). Measurements in 2% intralipid tissue phantoms reveal a sensitivity to ~30ppm nanorods when the density of the intralipid is randomized by 0.4% (or a fraction of 0.2). This has application toward molecular imaging using targeted nanorods within densely scattering, inhomogeneous tissues.

Keywords: optical coherence tomography, contrast agents, plasmon-resonance, albedo

*boppart@uiuc.edu; phone 1 217 244-7479; http://bil.nb.uiuc.edu/biophotonics/

1. INTRODUCTION

There has been much recent interest in developing contrast agents for optical coherence tomography (OCT),[1] analogous to the use of fluorescent markers in microscopy. One class of potential contrast agents includes gold nanoparticles, which exhibit low cytotoxicity for medical use.[2-4] Gold nanoparticles are optically interesting because they are known to exhibit the phenomenon of surface plasmon resonance, where optical excitation results in collective behavior of electrons, resulting in strong optical extinctions. Gold nanospheres have been developed as optical contrast agents. However, they exhibit resonances at shorter wavelengths than the near-infrared (NIR) region, which is preferred for biological imaging. The use of rod-like gold particles, known as nanorods, are known to increase the SPR into the NIR. In particular it was found that the aspect ratio of the rod (length-to-width) is related to the resonance wavelength in a monotonically increasing fashion.[5] Also it is known that smaller rods (<100nm) are dominated by absorption, whereas larger rods exhibit significant scattering, as predicted by Rayleigh theory.[6] Small, absorbing nanoparticles are of particular interest for hyperthermic therapy, where high intensity light is used to deliver heat via the nanoparticles, resulting in targeted cell killing.[7] This was recently demonstrated by targeted therapy with nanorods.[8] Also, the chemical pathways for functionalizing gold surfaces with proteins for specific cell targeting are well-known.[9] Thus, gold nanoparticles, and nanorods in particular, hold much promise toward biomedical imaging and therapy applications.

Other plasmon-resonant structures have recently been investigated as OCT contrast agents. Nanoshells consist of a silica core and gold shell, and based on the core/shell thickness can be designed for a specific resonance wavelength[10] and albedo.[11] However, many of the nanoshells investigated to date require larger diameters (>200nm) to provide OCT contrast,[12] which may limit their *in vivo* mobility and biodistribution. Another promising structure are gold nanocages, which consist of hollowed-out cubes with ~35nm dimensions, and exhibit a resonance near 800nm.[13] These were detected in OCT images within scattering tissue phantoms using spectroscopic OCT to sense

Coherence Domain Optical Methods and Optical Coherence Tomography in Biomedicine XI
edited by James G. Fujimoto, Joseph A. Izatt, Valery V. Tuchin
Proc. of SPIE Vol. 6429, 64291Z, (2007) · 1605-7422/07/$18 · doi: 10.1117/12.702847

the absorption band, which was tuned to the shorter wavelengths of the OCT light spectrum.[14] One problem with all of these structured SPR nanoparticle constructs is size or shape dispersity (inhomogeneity) which result in a broadening and concomitant reduction of the peak of the spectral response. Sharper peaks would increase the imaging sensitivity using spectroscopic OCT or related techniques.[15] Nanorods in particular are synthesized by a variety techniques, ranging from template-based growth to higher-yield batch processes, with recent emphasis on size monodispersity.[16] In particular, various seed-mediated growth methods using a CTAB (cetyl-trimethylammonium bromide) surfactant have been employed to achieve nanorods with aspect ratios from 1.5-10 with widths controllable from 6 to 12 nm,[17] and aspect ratios up to 20 have been reported with ~90% yield.[18]

Here we investigate the use of gold nanorods prepared using a seeded surfactant technique with sulfide arrest in order to stabilize their optical response for long (> 1 year) shelf lives.[19] The nanorods are tuned to 800nm and investigated in tissue phantoms with OCT imaging. An albedo-based method for their detection[20] is used to take advantage of their dominant absorption property.

2. THEORY

2.1 Plasmon Resonance

According to electromagnetic theory,[6, 21] the aspect ratio and volume are the two most important geometrical parameters for predicting the optical response from ellipsoids. This can be seen by writing the absorption coefficient μ_a per unit fractional volume:

$$\frac{\mu_a}{NV_p} = \frac{2\pi}{3\lambda}\left(\varepsilon_m{}^{3/2}\varepsilon_2\right)F \tag{1}$$

and the scattering coefficient μ_s per fractional volume:

$$\frac{\mu_s}{NV_p} = \frac{8\pi^3 V_p}{9\lambda^4}\left[\varepsilon_m{}^2\left(\varepsilon_2{}^2 + (\varepsilon_1 - \varepsilon_m)^2\right)\right]F \tag{2}$$

where the factor F is given by a sum over the three principal axes:

$$F = \sum_{i=1..3} \frac{1}{L_i{}^2\left[\varepsilon_2{}^2 + \left(\varepsilon_1 + \varepsilon_m\left(\frac{1-L_i}{L_i}\right)\right)^2\right]} \tag{3}$$

with geometrical factors L_i (i=1,2,3):[6]

$$\begin{aligned} L_1 &= \left(\frac{1-e^2}{e^2}\right)\left[\frac{1}{2e}\ln\left(\frac{1+e}{1-e}\right) - 1\right] \\ L_2 &= L_3 = \frac{1-L_1}{2} \end{aligned} \tag{4}$$

and parameter e determined by the aspect ratio R:[6]

$$e = \sqrt{1 - \frac{1}{R^2}} \tag{5}$$

where N is the particle number density, λ the wavelength of incident light, ε_m the dielectric constant of the surrounding medium (assumed to be real only, that is, non-absorbing), and ε_1 and ε_2 are the real and imaginary parts of the particle dielectric constant, respectively. It is important to note that the result for μ_s is 3 times smaller than Eq. (43) in [21], which was verified based on the polarizabilities given in [6].

Comparing Eq. (1) and (2) we see that the scattering coefficient scales with the square of the particle volume, where the absorption coefficient scales linearly. Thus, the particle albedo $a = \mu_s/(\mu_s+\mu_a)$ increases with V_p. The longitudinal or transverse resonance conditions occur when the denominator in Eq. (3) approaches zero for i=1 or i=2,3, respectively, and thus are the same for both scattering and absorption. Because L_1 monotonically decreases with

increasing R, there is a unique aspect ratio that satisfies the resonance condition for a specific particle type and wavelength (*e.g.*, $\varepsilon_1(\lambda)$ and $\varepsilon_2(\lambda)$). Thus, in gold, which is highly dispersive at optical wavelengths, the resonance wavelength is effectively tuned by the choice of aspect ratio.

The above treatment is for pure ellipsoids, whereas real nanorods tend to have a shape more like a cylinder with hemispherical caps, or perhaps even a slightly enlarged endcap more like a dumbbell. This may result in a change in the resonance conditions. Also, the above electrostatic theory uses the Rayleigh approximation ($|n_p|d << \lambda$, n_p is the particle refractive index and d the diameter), which may not be valid for larger rods. However, experimental results to date have shown good agreement with the responses from smaller nanorods (widths < 20nm) and electrostatic theory.[5]

2.2 OCT Imaging

The importance of contrast agent albedo for OCT imaging can be understood in terms of the OCT signal amplitude S (the amplitude of the complex analytic continuation of the OCT interferogram). For a homogeneous medium and assuming no multiple scattering, this can then be written as follows:

$$S(z) = S_0 \sqrt{\mu_b} \exp(-\mu_t z) f(z - z_f) \tag{6}$$

where μ_b is the 180 degree backscattering coefficient of the medium, μ_t is the extinction coefficient of the medium ($\mu_t = \mu_a + \mu_s$), z is the depth below the tissue surface, S_0 is a system hardware-dependent scaling parameter, and f is a function (typically the square root of a Lorentzian)[22] which accounts for the loss of efficiency away from a fixed focus at depth z_f. The medium therefore determines the values of μ_b and μ_t, which are fitted from the acquired OCT data. The concentration of contrast agents can then be extracted from measurements of μ_b and μ_t given prior knowledge of the tissue parameters.

There are several issues which should be noted regarding Eq. (6). The assumption of no multiple scattering effectively means that the optical coefficients μ_b, *etc.*, scale linearly with the density of the medium (or analogously the concentration of endogenous scatterers or contrast agents). This means that medium density fluctuations can be corrected against by defining the backscattering albedo $a' = \mu_b / \mu_t$. As previously noted,[23] this parameter is only sensitive to the underlying cross-sections of the scatterers and independent of their density. However, the assumption of insignificant multiple scattering may not always be true for imaging biological tissues, in which case future analysis may require higher-order terms to be accounted for in correcting for density fluctuations.

Another important issue is the exact definition of the backscattering coefficient μ_b. OCT senses the backward-scattered light that is collected by the imaging optics, which is primarily dependent on the numerical aperture (NA). Thus, a more accurate definition of μ_b for Eq. (6) would be:

$$\mu_b = \mu_s \int_0^{\pi} \int_0^{2\pi} g(\theta,\phi) p(\theta,\phi) \cos\theta \, d\theta \, d\phi \tag{7}$$

where p is the phase function (angular scattering function) of the medium, and g is the collection efficiency of the OCT system for a given scattered light ray. However, for the smaller NAs typically used in OCT imaging, the 180 degree backscattering is a reasonable approximation of the expected response. The exact scaling of μ_b (that is, the solid angle over which μ_b is defined, such as for the "radar" backscattering coefficient) in practice is not tremendously important, as it can be encompassed by the hardware-dependent parameter S_0 in Eq. (6). Since the detection of contrast agents is done in a differential measurement, only relative changes in μ_b are important, and thus it is only necessary to calibrate the scale of μ_b for a given OCT imaging system. In terms of albedo (a number between 0 for pure absorption and 1 for pure scattering), we know that the backscattering is only a small fraction of the total scattering and thus typical values for a' should be <<1. However, for the reasons outlined above, a' is typically calibrated to be 1 for an unperturbed tissue, and thus modifications by the contrast agents raise or lower this value.

3. EXPERIMENTS AND RESULTS

Gold nanorods were synthesized from gold seeds (~3.5nm) by reducing $AuCl_4$ in the presence of CTAB.[19] Treatment with Na_2S halted the optical drift of the nanorods, after which nanorods were centrifuged and resuspended into water. The particular batch discussed in this manuscript was aged 9 months before characterization and imaging. A typical TEM image (Philips, CM200, FEI Company) is shown in Figure 1. TEM image analysis was performed where the long and short axes, l and w, respectively, of each distinct nanorod were measured (dense clumps of overlapping nanorods were not measured). The aspect ratio $R = l/w$ and particle volume $V_p = \pi(w/2)^2(l - w/3)$ (assuming the shape of a cylinder with hemispherical ends) were computed for each rod. The results of these measurements are displayed in Figure 2.

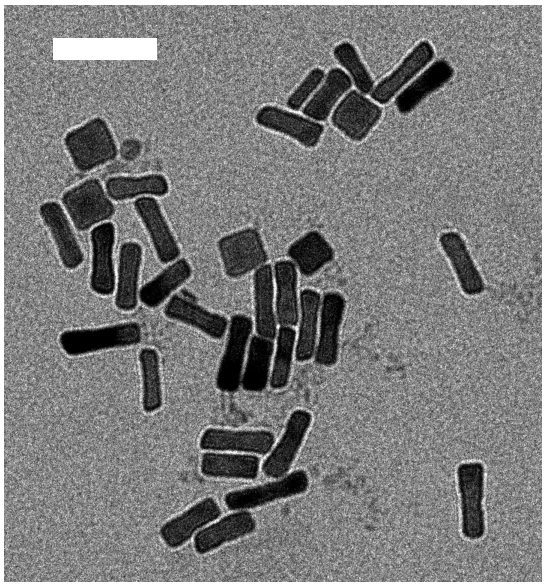

Fig. 1. Transmission electron micrograph (TEM) of gold nanorods, white scalebar 100nm.

The extinction spectrum of the nanorods were measured using a spectrophotometer (USB-ISS-VIS, Ocean Optics, Inc.) and is shown in Fig. 3. The fractional weight of gold was measured using mass spectrometry (ICP, OES Optima 2000 DV, Perkin Elmer). A corresponding theoretical absorption spectrum was computed using the nanorod size data of Fig. 2, as follows. First, the absorption coefficient of a single rod i of volume $V_{p,i}$ and aspect ratio R_i with density N_i is known from Eq. (1):

$$\mu_{a,i} = N_i V_{p,i} \frac{2\pi}{3\lambda}\left(\varepsilon_m^{3/2}\varepsilon_2\right)F(R_i) \tag{8}$$

Assuming independent scattering, the response from multiple nanorods is a linear sum:

$$\mu_{a,tot} = \sum_i \mu_{a,i} \tag{9}$$

The particle density N_i for each nanorod (i=1..1908) counted from the TEM images is equal, and thus we can write:

$$\sum_i N_i V_{p,i} = N\sum_i V_{p,i} = f_{vol} \tag{10}$$

where f_{vol} is the fractional volume occupied by the nanorods in the aqueous solution. Finally, f_{vol} is related to the fractional weight f_{wt} measured from mass spectrometry by $f_{vol} \cdot \rho_{Au} = f_{wt}$, where the density of gold ρ_{Au}=19.3 g/mL. Putting it all together:

$$\mu_{a,tot} = \frac{f_{wt}}{\rho_{Au}} \cdot \frac{2\pi\left(\varepsilon_m^{3/2}\varepsilon_2\right)}{3\lambda} \cdot \frac{\sum_i V_{p,i}F(R_i)}{\sum_i V_{p,i}} \tag{11}$$

Thus, Eq. (11) was used to compute $\mu_{a,tot}$ for each wavelength λ, using the wavelength-dependent dielectric constants $\varepsilon(\lambda)$ known for water[24] and gold.[25] A similar expression for the total scattering coefficient is obtained, allowing for computation of the extinction and also the albedo of the real nanorods solution.

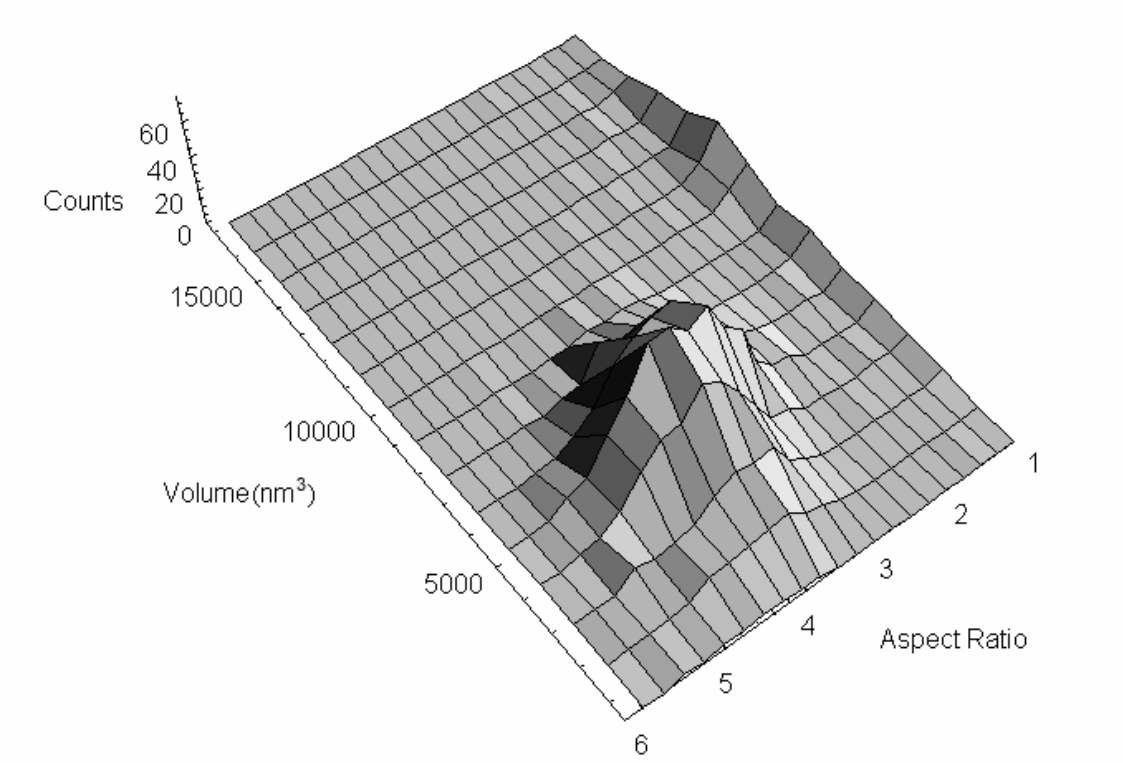

Fig. 2. Gold nanorod volume and aspect ratio distribution histogram (n=1908) determined from TEM. Note that two distinct populations are evident, one with a mean aspect ratio of 3.8, and a smaller population of cube-like particles (~10%).

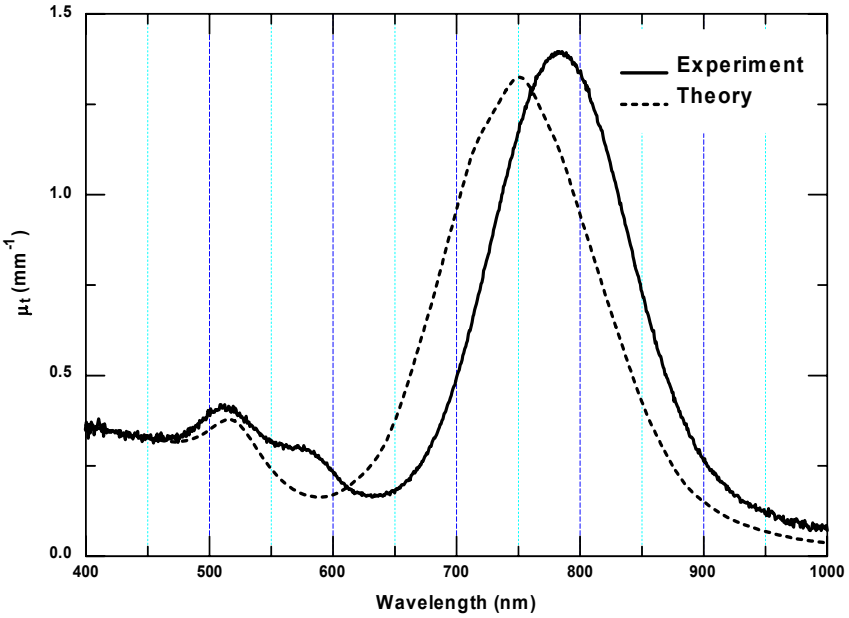

Fig.3. Extinction spectra of gold nanorods based on theoretical calculations and experimental measurements.

It was shown previously using double-integrating sphere measurements that these nanorods are low-albedo in the NIR.[26] This was also computed using the above theoretical analysis, predicting $a = 0.09$ at the longitudinal resonance. There is excellent agreement in Fig. 3 between theoretical and experimental spectra in both the absolute height and width of the plasmon resonance. The longitudinal resonance of the nanorods is peaked at 784 nm with a full-width at half-maximum of 135 nm, which is broadened due to dispersity in the nanorods' aspect ratios. The slight red-shift of the experimental response is possibly due to the CTAB capping material which has a higher refractive index than the surrounding water medium, which was not accounted for in the theoretical calculations. The extinction cross-section is estimated to be $\sim 1.3 \times 10^{-15}$ m^2. Although this is somewhat smaller than that reported for gold nanocages,[27] we estimate the surface area and volume of an individual nanorod to be ~6-7 × smaller than that of a nanocage. Linewidths below 100 nm and a simultaneous increase in cross-section may be achieved in future work by optimization of the seeded growth conditions.[28]

We performed Monte Carlo simulations to measure the sensitivity of contrast agent detection in a homogeneous tissue according to Eq. (6), where shot noise and noise in the underlying tissue medium concentration were added to simulate tissue fluctuations. The effect of the contrast agents were modeled as linearly modifying the extinction and backscattering coefficients. We found that contrast agents are most effective when they modify a' from that of the tissue medium, therefore contrast agents should be chosen to maximize $|a'_{\text{tissue}} - a'_{\text{contrast agent}}|$. In the usual case of highly forward-scattering tissue, this indicates the use of absorbing contrast agents with low a', or perhaps extremely highly backscattering agents which raise a' from that of the tissue. The latter case, however, is difficult to achieve in practice for nanosized particles, since the scattering coefficient scales as the square of the particle volume.

To demonstrate the importance of the backscattering albedo on contrast agent sensitivity, we measured the dose-response of low backscattering albedo nanorods within a 2% intralipid tissue phantom aqueous solution which exhibits a high backscattering albedo. Mixtures of nanorods and intralipid were imaged with an 800nm fiber-based OCT system with -100dB sensitivity and 10mW optical power at the sample, over a 2mm optical depth. The average depth-dependent OCT signal amplitude was computed, and μ_b and μ_t were fit using Eq. (6). We found that extremely small dosages of nanorods were required to modify the optical properties of the medium. Nanorods as doses of 100ppm, or a fractional volume of 0.0005%, were sufficient to lower a' by 20%, while simultaneously raising the extinction coefficient by 1mm^{-1} (from 3.5mm^{-1} to 4.5mm^{-1}). As a comparison, silica spheres (800nm diameter, Bangs Labs) were also mixed with intralipid and imaged in the same way. A fractional volume of 0.9% silica spheres was required to raise the extinction coefficient by 1mm^{-1}, and because they are less absorbing than the nanorods, a' was only reduced by 10%. This highlights the advantage of plasmon-resonant nanoparticles in reducing the necessary dosage required to produce contrast.

Next we investigated the detectability of nanorods within a medium with known average optical properties, but statistical fluctuations in the concentration of the medium. This was achieved by preparing a set of ten 2% ± 0.4% intralipid tissue phantoms from a randomly generated list of concentrations. Nanorods at a concentration of 80ppm were added to five sets, and five were unmodified as controls. OCT images were acquired as before, and fits of a' versus μ_t for each sample were measured. The results are displayed in Table 1. We see clearly that nanorod-doped phantoms exhibited a significant decrease in a', while fluctuations in μ_t were sufficiently large that modifications by the nanorods were insignificant. This emphasizes the importance of a' as a concentration-independent measure of the underlying scatterer cross-sections, for the detection of contrast agents. Based on statistics from these results, we estimate the nanorods detection threshold is ~30 ppm within the 2% intralipid solutions.

Sample	Extinction μ_t (mm^{-1})	Backscattering albedo a' (relative)
No nanorods	3.82 ± 0.11	0.990 ± 0.002
With nanorods	3.94 ± 0.24	0.761 ± 0.008

Table 1. Comparison of the mean ± standard deviation of μ_t and a' measured from OCT images within 2 ± 0.4% intralipid solutions with and without added nanorods (n=5).

4. CONCLUSIONS

Nanorods are promising for *in vivo* applications because it has been shown that with appropriate surface coatings they do not exhibit cytotoxicity at concentrations of 30ppm.[2-4] Also, functionalization of the nanorods for cell surface receptor targeting may be possible, because, given an average cell size of 10 μm, this concentration corresponds to approximately 140 nanorods per cell. The ability to detect nanorods within real tissues with inhomogeneities and to provide concentration maps within tissues remains to be shown, however, by modifying Eq.(6) to account for depth-dependent μ_t and μ_b. Further improvements in sensitivity may be achieved by combining these backscattering albedo measurements with spectroscopic OCT to detect the nanorod-specific resonance. Using OCT to image the targeting of nanorods *in vivo* may ultimately aid in the development of photothermal therapies, where the highly absorbing nanorods provide site-specific hyperthermia.[8]

REFERENCES

1. S. A. Boppart, A. L. Oldenburg, C. Xu, D. L. Marks, "Optical probes and techniques for molecular contrast enhancement in coherence imaging", J. Biomed. Opt. **10**, 041208 (2005).
2. Y. Zhao, B. Sadtler, M. Lin, G. H. Hockerman, A. Wei, "Nanoprobe implantation into mammalian cells by cationic transfection", Chem. Commun. pp.784 (2004).
3. E. E. Connor, J. Mwamuka, A. Gole, C. J. Murphy, M. D. Wyatt, "Gold nanoparticles are taken up by human cells but do not cause acute cytotoxicity", Small **1**(3), 325 (2005).
4. H. Takahashi, Y. Niidome, T. Niidome, K. Kaneko, H. Kawasaki, S. Yamada, "Modification of gold nanorods using phosphatidylcholine to reduce cytotoxicity", Langmuir **22**(1) 2 (2006).
5. S. Link, M. B. Mohamed, M. A. El-Sayed, "Simulation of the optical absorption spectra of gold nanorods as a function of their aspect ratio and the effect of the medium dielectric constant", J. Phys. Chem. B **103**, 3073 (1999).
6. C. F. Bohren and D. R. Huffman, *Absorption and Scattering of Light by Small Particles*, pp. 141 (John Wiley and Sons, 1983).
7. L. R. Hirsch, R. J. Stafford, J. A. Bankson, S. R. Sershen, B. Rivera, R. E. Price, J. D. Hazle, N. J. Halas, J. L. West, "Nanoshell-mediated near-infrared thermal therapy of tumors under magnetic resonance guidance," Proc. Natl. Acad. Sci. USA **100**, 13549 (2003).
8. X. Huang, I. H. El-Sayed, W. Qian, M. A. El-Sayed, "Cancer cell imaging and photothermal therapy in the near-infrared region by using gold nanorods," J. Am. Chem. Soc. **128**, 2115 (2006).
9. C. M. Niemeyer, "Nanoparticles, proteins, and nucleic acids: Biotechnology meets materials science," Angew. Chem. Int. Ed. **40**, 4128 (2001).
10. S. J. Oldenburg, R. D. Averitt, S. L. Westcott, N. J. Halas, "Nanoengineering of optical resonances," Chem. Phys. Lett. **288**, 243 (1998).
11. C. Loo, A. Lin, L. Hirsch, M.-H. Lee, J. Barton, N. Halas, J. West, R. Drezek, "Nanoshell-enabled photonics-based imaging and therapy of cancer," Tech. in Canc, Res. and Treat., **3**, 33 (2004).

12. A. Agrawal, S. Huang, A. W. H. Lin, M.-H. Lee, J. K. Barton, R. A. Drezek, T. J. Pfefer, "Quantitative evaluation of optical coherence tomography signal enhancement with gold nanoshells," J. Biomed. Opt. **11**, 041121 (2006).

13. J. Chen, F. Saeki, B. J. Wiley, H. Cang, M. J. Cobb, Z.-Y. Li, L. Au, H. Zhang, M. B. Kimmey, X. Li, Y. Xia, "Gold nanocages: bioconjugation and their potential use as optical imaging contrast agents," Nanolett. **5**, 473 (2005).

14. H. Cang, T. Sun, Z.-Y. Li, J. Chen, B. J. Wiley, Y. Xia, X. Li, "Gold nanocages as contrast agents for spectroscopic optical coherence tomography," Optics Lett. **30**, 3048 (2005).

15. K. Chen, Y. Liu, G. Ameer, V. Backman, "Optimal design of structured nanospheres for ultrasharp light-scattering resonances as molecular imaging multilabels," J. Biomed. Opt. **10**, 024005 (2005).

16. J. Perez-Juste, I. Pastoriza-Santos, L. M. Liz-Marzan, P. Mulvaney, "Gold nanorods: Synthesis, characterization and applications," Coord. Chem. Rev. **249**, 1870 (2005).

17. B. Nikoobakht, M. A. El-Sayed, "Preparation and growth mechanism of gold nanorods (NRs) using seed-mediated growth method," Chem. Mater. **15**, 1957 (2003).

18. B. D. Busbee, S. O. Obare, C. J. Murphy, "An improved synthesis of high-aspect-ratio gold nanorods," Adv. Mater. **15**, 414 (2003).

19. D. A. Zweifel and A. Wei, "Sulfide-arrested growth of gold nanorods," Chem. Mater. **17**, 4256 (2005).

20. A. L. Oldenburg, M. N. Hansen, D. A. Zweifel, A. Wei, S. A. Boppart, "Plasmon-resonant nanorods as low backscattering albedo contrast agents for optical coherence tomography," Opt. Express **14**, 6724 (2006).

21. G. C. Papavassiliou, "Optical properties of small inorganic and organic metal particles," Prog. Solid St. Chem. **12**, 185 (1979).

22. T. G. van Leeuwen, D. J. Faber, M. C. Aalders, "Measurement of the axial point spread function in scattering media using single-mode fiber-based optical coherence tomography," IEEE J. Sel. Top. Quantum Electron. **9**, 227 (2003).

23. J. M. Schmitt, A. Knuttel, R. F. Bonner, "Measurement of optical properties of biological tissues by low-coherence reflectometry," Appl. Opt. **32**, 6032 (1993).

24. P. D. T. Huibers, "Models for the wavelength dependence of the index of refraction of water," Appl. Opt. **36**, 3785 (1997).

25. P. B. Johnson, R. W. Christy, "Optical constants of the noble metals," Phys. Rev. B **6**, 4370 (1972).

26. A. L. Oldenburg, D. A. Zweifel, C. Xu, A. Wei, S. A. Boppart, "Characterization of plasmon-resonant gold nanorods as near-infrared optical contrast agents investigated using a double-integrating sphere system," Proc. SPIE **5703**, 50 (2005).

27. J. Chen, B. Wiley, Z.-Y. Li, D. Campbell, F. Saeki, H. Cang, L. Au, J. Lee, X. Li, Y. Xia, "Gold nanocages: engineering their structure for biomedical applications," Adv. Mater. **17**, 2255 (2005).

28. M. Liu, P. Guyot-Sionnest, "Mechanism of silver(I)-assisted growth of gold nanorods and bipyramids," J. Phys. Chem. B **109**, 22192 (2005).